



# Corrosion Resistance, Mechanical and Magnetic Properties of Cold-Sprayed Al Coating on Sintered NdFeB Magnet

Yuanming Gao<sup>1</sup> · Yu Bai<sup>1</sup> · Hao Zhu<sup>1</sup> · Weicheng Liang<sup>1</sup> · Qi Liu<sup>1</sup> · Hongying Dong<sup>2</sup> · Ruiling Jia<sup>1</sup> · Wen Ma<sup>1</sup>

Submitted: 22 July 2021 / in revised form: 23 September 2021 / Accepted: 3 October 2021 / Published online: 17 November 2021  
© ASM International 2021

**Abstract** A protective aluminum coating was deposited by cold spray on the surface of a sintered neodymium substrate ( $\text{Nd}_2\text{Fe}_{14}\text{B}$ ) made from an alloy of neodymium, iron, and boron and used as a permanent magnet. Most of the sprayed aluminum particles softened and deposited onto the substrate, forming a uniform and dense coating with a thickness of about 45  $\mu\text{m}$ . The bonding strength and Vickers hardness of the coating were 26.0 MPa and 7.02 GPa, respectively. The corrosion current ( $I_{\text{corr}}$ ) densities of the sintered NdFeB with and without the aluminum coating in 3.5 wt.% NaCl solution were  $3.847 \times 10^{-5} \text{ A/cm}^2$  and  $3.866 \times 10^{-4} \text{ A/cm}^2$ , respectively. The sintered NdFeB with the protective aluminum coating survived up to 200 h in the neutral salt spray test (NSS). Its coercivity, remanence, and maximum energy product were 14.813 kOe, 13.994 kGs, and 46.798 MGOe, respectively. They were lower than that of the substrate without coating by 2.94%, 0.03%, and 1.69%. This study showed that the aluminum coating prepared by cold spray could effectively increase the corrosion resistance of the sintered NdFeB magnet with a weak effect on its magnetic properties.

**Keywords** aluminum coating · cold spray · magnetic property · NdFeB · neodymium

✉ Yu Bai  
18847123425@163.com

✉ Wen Ma  
wma66@163.com; wma@imut.edu.cn

<sup>1</sup> Inner Mongolia Key Laboratory of Thin Film and Coatings, School of Materials Science and Engineering, Inner Mongolia University of Technology, Hohhot 010051, China

<sup>2</sup> School of Chemical Engineering, Inner Mongolia University of Technology, Hohhot 010051, China

## Introduction

Sintered NdFeB (S-NdFeB) magnet is a new generation of permanent magnetic materials, with small size, light-weight, strong magnetic and other characteristics, known as the king of magnets (Ref 1). With ever increasing demands of electronics, acoustics, automation, communications, and magnetic resonance imaging for magnetic materials, the S-NdFeB has become the most widely used permanent magnetic material in the world recently (Ref 2). However, due to existence of the low potential of Nd-rich phase in the S-NdFeB, intercrystalline corrosion is prone happen, which limits its use in high temperature, humid hot and corrosive environment (Ref 3-6). Therefore, it is very important to improve the corrosion resistance of the S-NdFeB.

The corrosion resistance of the S-NdFeB can be improved by adding alloys or applying coatings (polymer or metals) (Ref 7-9). However, adding alloys result in an excessive magnetic loss, while applying polymer coating cannot meet the demands of the high-performance S-NdFeB. Thus, metallic coating prepared by different techniques is the main way to improve the corrosion resistance of the S-NdFeB (Ref 10, 11). Corrosion-resistant metal coatings on the S-NdFeB surface can be prepared by electroplating, electroless plating, ion plating and magnetron sputtering (Ref 12-15).

In recent years, cold spray has been considered as a new coating preparation technology, because the cold-sprayed metallic coatings have low grain growth rate and oxidation rate, which are also compact with low porosity (Ref 16). These process advantages make cold spray particularly suitable for depositing anticorrosion coatings of many metallic parts such as cylinders, turbine blades and pistons (Ref 17). In addition, the cold-sprayed metallic coatings

**Table 1** Chemical compositions of the S-NdFeB

Chemical compositions	Nd	Fe	B	Others (Dy, Tb, Co, Go, Al, Cu, etc.)
Weight percent, %	32	64	1	3

form at low temperatures in comparison with other processes with tailored microstructures (Ref 18). The cold spray equipment is low cost and environmental friendly, so the coatings prepared by cold spray can meet the requirements in terms of economy, environmental protection and performance (Ref 19–21). Kuroda et al. studied the aluminum (Al) and Zn–Al coatings of 175  $\mu\text{m}$  thickness on surface of steel pipes for the 18-year marine field test, and found the coatings maintain their superb corrosion protection under such severe conditions (Ref 22). Chen et al. reported that the Al coating acts as a sacrificial layer, which provides a better corrosion-wear resistance for the substrate compared to the traditional Zn coating in saline solution (Ref 23). In addition, Al is a kind of active metal, and it easily reacts with  $\text{O}_2$  to form  $\text{Al}_2\text{O}_3$  in the air.  $\text{Al}_2\text{O}_3$  is very dense film, it can separate the metal substrate from outside environment completely. In general, Al often protects metals from corrosion as corrosion inhibitors (Ref 24).

In this work, the S-NdFeB magnets were coated with Al coating by cold spray, and the corrosion behavior of the Al-coated S-NdFeB magnets in NaCl solution as well as their mechanical and magnetic properties were studied.

## Experimental Procedure

The S-NdFeB specimens (N50, Baotou Jinneng Magnetic Materials Co. Ltd, Baotou, China) with a size of 20 mm  $\times$  15 mm  $\times$  5 mm and  $\Phi$ 25 mm  $\times$  5 mm were used as substrates in this work. The chemical compositions of the S-NdFeB are listed in Table 1. The surface morphology of the S-NdFeB used in the experiment is shown in Fig. 1 (a). All specimens were demagnetized and roughened by grit blasting using  $\text{Al}_2\text{O}_3$  24# grit, followed by ultrasonic cleaning using ethanol, pickling with nitric acid and activating with citric acid successively.

Industrial pure Al powder (99.81 wt.%) (Jinhao New Materials Technology Co. Ltd, Hunan, China) produced by nitrogen atomization was used as a feedstock material for spraying Al coating. The morphology of the Al powder used in the experiment is shown in Fig. 1(b). The most of the powders are spherical shape with the diameters in the range of 20 to 45  $\mu\text{m}$ .

The deposition of Al coating was carried out by cold spray apparatus (LP-TCY-II, Beijing Tianchengyu New Materials Technology Co. Ltd, Beijing, China), which is attached to a robotic arm. The spray parameters are listed in Table 2.

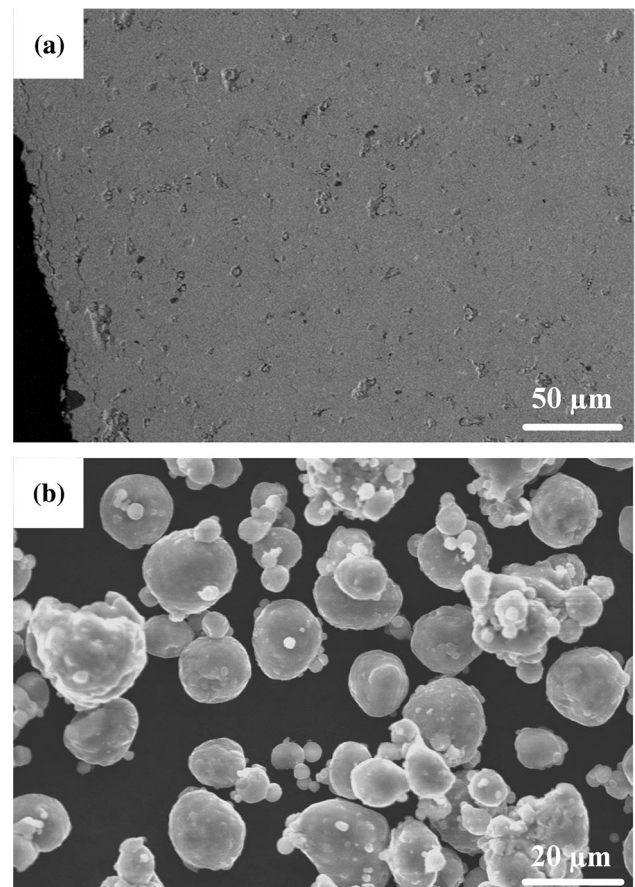


**Fig. 1** Surface morphology of the S-NdFeB (a) and microstructure of the Al powder (b)

The phase structure of the Al powder and Al coating was analyzed by x-ray diffraction (XRD, Model D/Max 2500PC Rigaku, Japan) operated at 45 kV and 200 mA with  $\text{Cu K}_\alpha$  radiation at a scanning rate of 3°/min, over the range of 20° to 80°. The surface and cross-section microstructure analyses of the Al coating were carried out using a scanning electron microscopy (SEM, Model S-3400N Hitachi, Japan) with energy dispersive spectrometer (EDS, Model Inca, Oxford Instruments, Oxfordshire, United Kingdom).

The corrosion behavior of the S-NdFeB coated with Al coating was determined by potentiodynamic polarization and electrochemical impedance spectroscopy (EIS, Model PP211 ZAHNER, Germany) tests using a classical three electrodes system in 3.5 wt.% deoxidized NaCl solution at room temperature. The reference electrode and counter electrode were saturated calomel (SCE) and platinum electrode, respectively. The electrolyte solution is HCl

**Table 2** Cold spray parameters of the Al coating

Spray pressure, MPa	Spray temperature, °C	Spray distance, mm	Raster scan step size, mm	Gun movement rate, mm/s	Powder feeding rate, g/min	Coating thickness, $\mu\text{m}$
1.0	150	10	0.4	750	1.87	45

(2 mol/L), and the test time of the open-circuit potential (OCP) is 5 min. The Al coating or S-NdFeB was used as a working electrode. And the surface area of the specimens exposed for corrosion study was  $0.283 \text{ cm}^2$ . The EIS measurements were carried out with signal amplitude of 5 mV and frequency range from  $10^5$  to  $10^{-2}$  Hz.

According to the international standard ISO 3768-1976, Metal Coating Neutral Salt Spray test (NSS test), the NSS test was carried out using atomized salt water (NaCl,  $(5 \pm 0.5)$  wt.%, pH 6.5-7.2) at temperature of  $(35 \pm 2)$  °C and humidity greater than 95%, with the fog reduction quantity of 1-2 ml/(h  $\text{cm}^2$ ), under the nozzle pressure of 78.5-137.3 kPa (0.8-1.4  $\text{kgf/cm}^2$ ).

The “pull-off” test was used for coating-substrate bond strength determination according to the GB/T 8642-2002 standard. The Al coating was sprayed on one end of the S-NdFeB ( $\Phi 25 \text{ mm} \times 5 \text{ mm}$ ), followed by bonding the Al-coated S-NdFeB in both surfaces with steel bar using E7 glue. The “pull-off” tests of the bonded samples were carried out after curing at 120 °C for 8 h with an elongation rate of 1.5 mm/min.

The hardness of the Al coating was measured by conventional hardness tester (Model HXD-1000TM/LCD, Shanghai Taiming Optical Instrument Co. Ltd, Shanghai, China) with applied load of 5 N and holding time of 10 s. Ten indents were performed on each sample to reduce the experimental uncertainty.

Magnetic properties of the sintered NdFeB with and without Al coating were characterized by magnetic properties tester (The HyMPulse magnetic properties tester, METIS, Belgium).

## Results and Discussion

### Microstructure and Composition Characterization

Compared with Fig. (1), Fig. 2(a) shows that the Al particles become oblate spheres and stack together, which are attributed to the impact of high-pressure airflow during cold spray process. It is shown in Fig. 2(b) that the Al coating is very dense, and no visible cracks appear at the interface. Lots of Al particles soften and stack quickly onto the NdFeB substrate, and plastically deformed Al particles

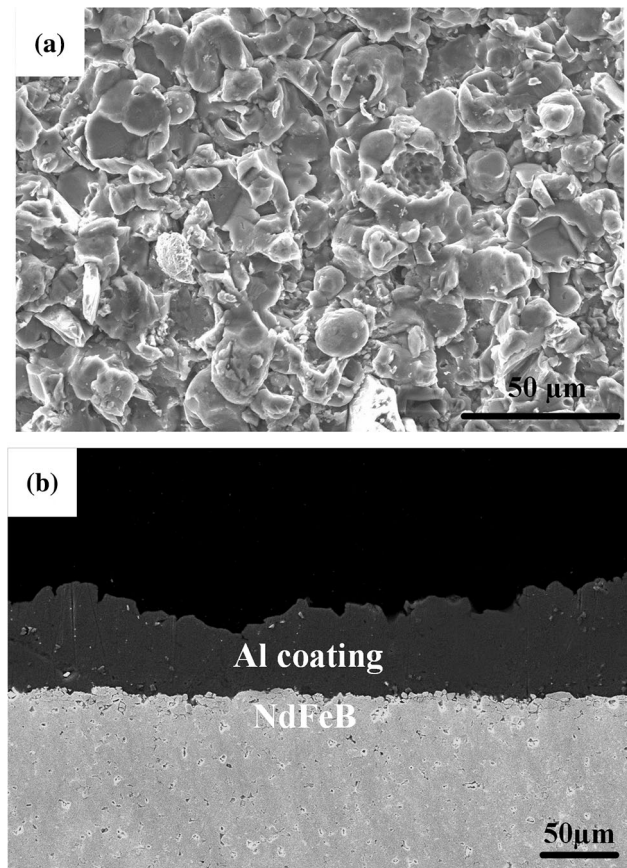


**Fig. 2** Surface microstructure (a) and cross-section microstructure (b) of the Al-coated S-NdFeB

form uniform and dense Al coating by mechanical bite force.

The XRD patterns of the Al powder and Al coating are shown in Fig. 3. The Al coating is prepared and stored in the air at room temperature. The phase compositions both of Al powder and Al coating are the same, indicating that the Al particles are not oxidized during the cold spray process.

### Corrosion Resistance

#### Potentiodynamic Polarization Curves

The potentiodynamic polarization curve mainly includes corrosion potential and corrosion current density. From the



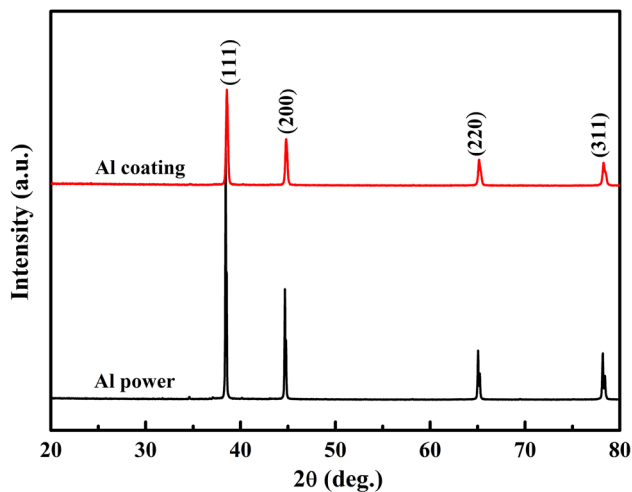


**Fig. 3** XRD patterns of the Al powder and cold-sprayed Al coating

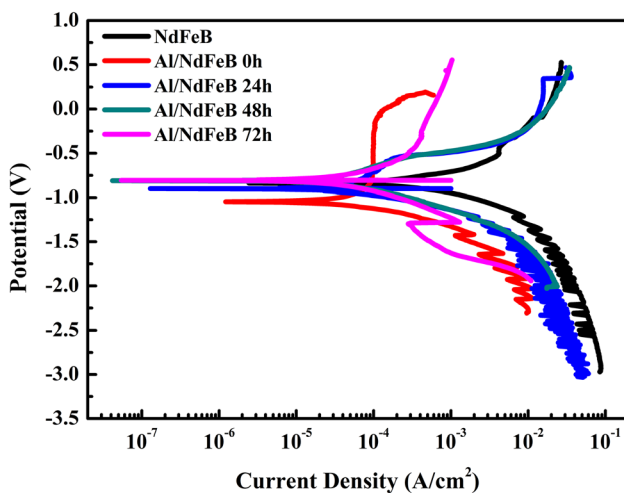


**Fig. 4** Potentiodynamic polarization curves of the S-NdFeB and Al-coated S-NdFeB with different immersion times in 3.5 wt.% NaCl solution

thermodynamic point of view of material corrosion, the corrosion potential is mainly concerned. The corrosion potential is more positive, the smaller the corrosion tendency is. Whereas from the perspective of corrosion dynamics of materials, the corrosion current density is mainly concerned. In particular, when evaluating the corrosion resistance of active dissolved materials, the primary parameter is corrosion current density. The corrosion current density is smaller, the corrosion resistance of materials will be the better (Ref 25).

Figure 4 shows the potentiodynamic polarization curves of the S-NdFeB and Al-coated S-NdFeB with different immersion times in 3.5 wt.% NaCl solution. Corrosion potential of the Al-coated S-NdFeB/0h is more negative than that of the S-NdFeB, indicating that the  $\text{Al}_2\text{O}_3$  film on the Al coating surface is damaged and more easily

**Table 3** Electrochemical parameters of the S-NdFeB and Al-coated S-NdFeB calculated from the potentiodynamic polarization curves in Fig. 4

Specimen	Immersion time, h	$E_{\text{corr}}$ , V	$I_{\text{corr}}$ density, $\text{A}/\text{cm}^2$
NdFeB	0	-0.839	$3.866 \times 10^{-4}$
Al/NdFeB	0	-1.044	$3.847 \times 10^{-5}$
Al/NdFeB	24	-0.894	$3.887 \times 10^{-5}$
Al/NdFeB	48	-0.812	$2.839 \times 10^{-5}$
Al/NdFeB	72	-0.803	$2.587 \times 10^{-5}$

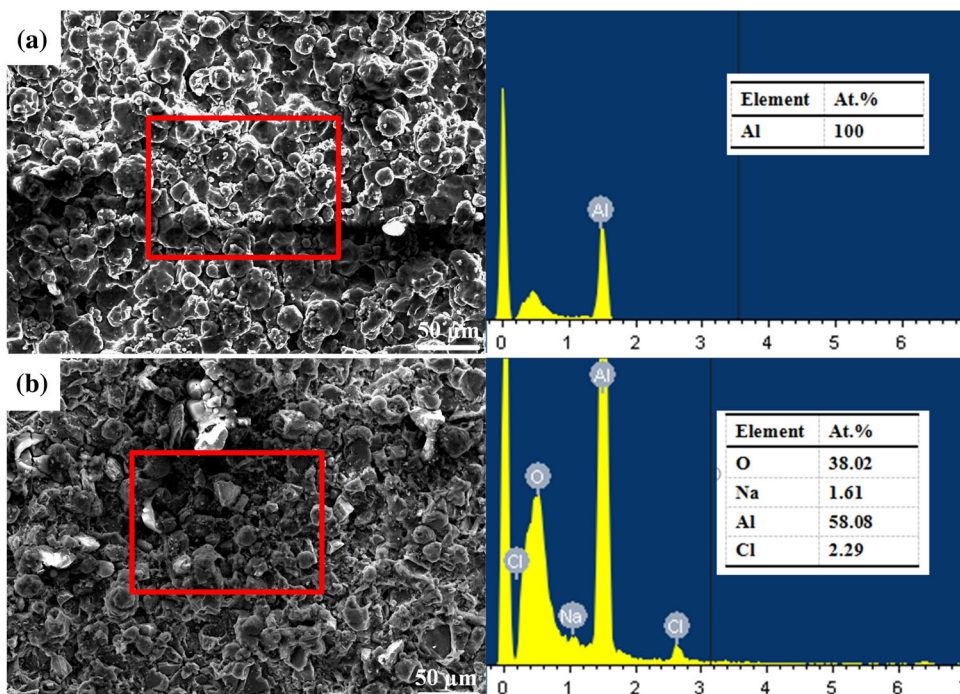
corroded. Al-coated S-NdFeB with 24, 48 and 72 h immersion time, a new substance is formed on the surface of the coating. The corrosion products hinder the corrosion, so there is a certain increase in corrosion potential. There is no significant difference in the shape of the potentiodynamic polarization curves of the Al-coated S-NdFeB with different immersion times. The cathodic polarization reactions are typical depolarization reactions of oxygen, and the second half is higher than the first half in the polarizability of anodic polarization curve. S-NdFeB and Al-coated S-NdFeB with different immersion times have certain anodic passivation phenomenon. The passivation of Al-coated S-NdFeB is mainly caused by surface oxidation, mainly due to the reaction of Al element. After that, the current increases rapidly with the potential, that is, an obvious overpassivation phenomenon. The anode reaction is controlled by diffusion, and the corrosion rate of the specimens decreased due to an obvious protective effect of Al coating on S-NdFeB.

Corrosion potential and corrosion current density of the S-NdFeB and Al-coated S-NdFeB are listed in Table 3. Corrosion current density of the S-NdFeB is  $3.866 \times 10^{-4} \text{ A}/\text{cm}^2$ , that is, higher than that of the as-sprayed Al-coated S-NdFeB ( $3.847 \times 10^{-5} \text{ A}/\text{cm}^2$ ), indicating that the Al coating can effectively decrease corrosion rate, and it protects S-NdFeB from corrosion in 3.5 wt.% NaCl solution.

After immersion in 3.5 wt.% NaCl solution for 24 h, the corrosion potential of the Al-coated S-NdFeB is more positive than that of the as-sprayed Al-coated S-NdFeB, that is, attributed to the development of oxides on the surface of the Al-coated S-NdFeB. However, corrosion current density of the Al-coated S-NdFeB after immersion for 24 h is higher than that of the as-sprayed Al-coated S-NdFeB due to the degradation of oxide film, resulting in a higher electrode polarization current density (Ref 26).

The corrosion current density of the Al-coated S-NdFeB decreases with further extending immersion time up to 48 h and 72 h. It implies that the developed oxides on the surface of the Al-coated S-NdFeB can decrease corrosion rate,

**Fig. 5** Surface microstructures and EDS analyses of the Al-coated S-NdFeB in as-sprayed state (a) and after corrosion in 3.5 wt.% NaCl solution (b)



and it can provide adequate cathodic protection for S-NdFeB.

The reason of the higher corrosion resistance for the Al-coated S-NdFeB in 3.5 wt.% NaCl solution can be explained as follows. Al reacts with O<sub>2</sub> and H<sub>2</sub>O to form Al(OH)<sub>2</sub> first and attach to the coatings surface (Eq 1), then Al(OH)<sub>2</sub> loses its H<sup>+</sup> and form AlOOH (Eq 2), and AlOOH decomposes into Al<sub>2</sub>O<sub>3</sub> and H<sub>2</sub>O finally (Eq 3). Figure 5 shows the surface microstructures and EDS analyses of the Al-coated S-NdFeB in as-sprayed state and after corrosion in 3.5 wt.% NaCl solution. Figure 6 shows XRD patterns of Al-coated S-NdFeB after corrosion in 3.5 wt.% NaCl solution. Before electrochemical test, the data of EDS and XRD show that the main component of the coating is Al, whereas the main component of the coating is Al<sub>2</sub>O<sub>3</sub> after electrochemical test. The results show that the inference of the whole reaction process is reasonable. During the whole reaction, both intermediate Al(OH)<sub>2</sub>, AlOOH and final product Al<sub>2</sub>O<sub>3</sub> are high impedance substances, resulting in no obvious galvanic corrosion even at a certain driving potential. The development of Al<sub>2</sub>O<sub>3</sub> on the surface of the Al-coated S-NdFeB becomes a barrier that delays the penetration of the corrosion electrolyte, achieving good corrosion resistance (Ref 15, 26, 27).

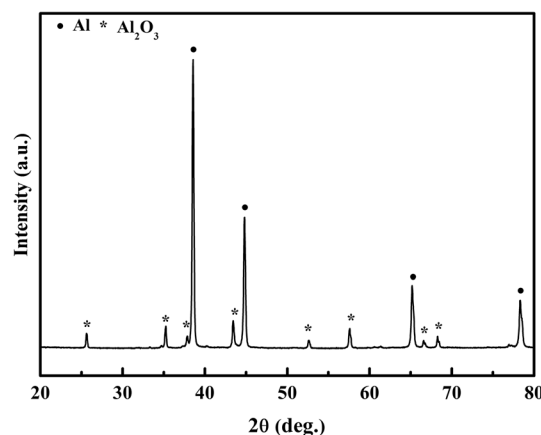


**Fig. 6** XRD patterns of the Al-coated S-NdFeB after corrosion in 3.5 wt.% NaCl solution

*Electrochemical Impedance Spectroscopy (EIS)*

Nyquist plots of the S-NdFeB and Al-coated S-NdFeB with different immersion times in 3.5 wt.% NaCl solution are shown in Fig. 7. The Nyquist plots of the S-NdFeB contain a high-frequency reactive arc and a low-frequency reactive arc, while the Al-coated S-NdFeB only contains a high-frequency reactive arc at the beginning of immersion, whereas the low-frequency diffusion arc reflects diffusion process from the corrosion products to corrosive medium or Cl<sup>-</sup>. The existence of inductive arc of the S-NdFeB indicates that pitting corrosion of the S-NdFeB more easily occurs than the Al-coated S-NdFeB.

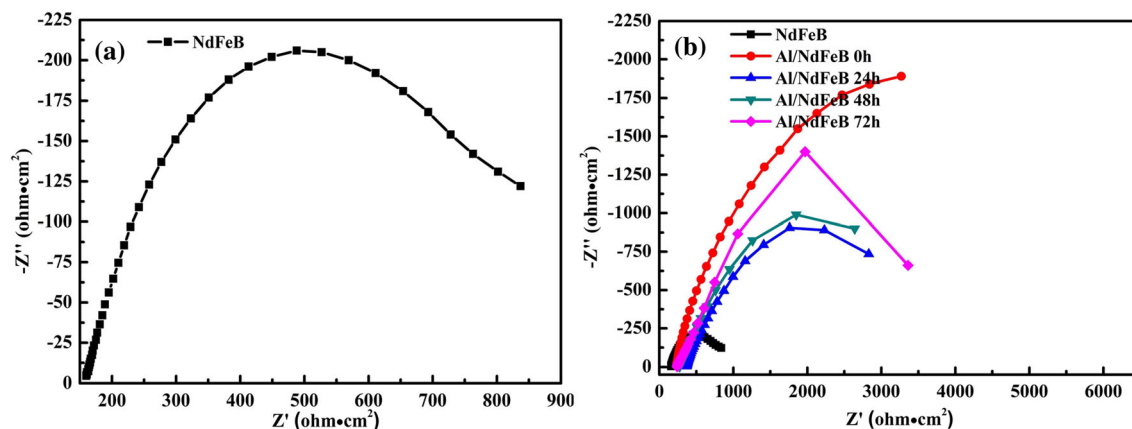


**Fig. 7** Nyquist plots of the S-NdFeB and Al-coated S-NdFeB with different immersion times in 3.5 wt.% NaCl solution

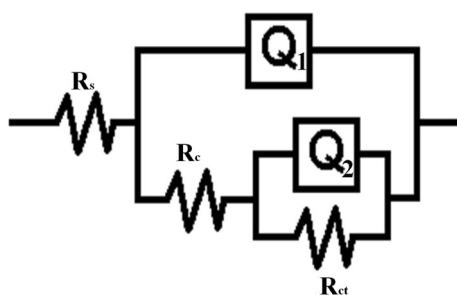


**Fig. 8** Equivalent circuits for EIS data

The arc curves indicate that the electron transfer process on the electrode surface is subject to impedance. The capacitive reactance arc radius of Al-coated S-NdFeB is much larger than that of S-NdFeB, which indicates that the charge transfer resistance is obviously increased with the enhanced corrosion resistance.

With the increase in immersion time, the capacitive reactance arc radius of Al-coated S-NdFeB is contraction, indicating that the charge transfer resistance of Al-coated S-NdFeB decreases. The capacitive reactance arc radius of immersion 24 h is smaller than immersion 48 h and 72 h, which is related to the change of the Al coating, charge transfer resistance of Al coatings increases with the decrease in the first reaction in the process of immersion, the decrease is formed from destruction of the oxide film in solution. After immersion time extended, the surface coatings form new oxide film to protect NdFeB substrate. In order to discuss the corrosion mechanisms clearly, Fig. 8 shows the equivalent circuits. The models are obtained after fitting the data from Nyquist diagrams by the ZsimpWin software (Ref 28, 29). The constant phase angle element (CPE, designated as Q) is used instead of the pure capacitance, and its admittance ( $Y_Q$ ) can be expressed as (Ref 30):

$$Y_Q = Y_0(\omega j)^n \quad (\text{Eq 4})$$

where  $Y_0$  is the admittance constant and  $n$  is the empirical exponent of the CPE,  $\omega$  is the angular frequency, and  $j$  is the imaginary number, respectively.

According to the previous studies of equivalent circuit for oxide films on metals (Ref 31–33), the model  $R(Q(R(QR)))$  (Fig. 8) is employed to simulate the Nyquist plots (0–72 h). In the equivalent circuit shown in Fig. 8,  $R_s$  represents the solution resistance,  $Q_1$  represents the oxide film capacitance,  $R_c$  is the electrical resistance to the ionic current through the defects in the Al oxide film,  $Q_2$  is the double-layer capacitance of electrochemical reaction, and  $R_{ct}$  is the charge transfer resistance. The fitted results are listed in Table 4. Table 4 shows that the simulated values of  $R_{ct}$  (24 h) decrease due to the effect of the pitting corrosion. The values of  $R_{ct}$  (48, 72 h) gradually increase and are larger than that of the  $R_{ct}$  of Al coating immersing for 24 h, which suggests that after immersing for 48 and 72 h, a stable barrier gradually forms on the surface of the Al coating and then prevents the solution ion penetration effectively. This result agrees well with the potentiodynamic polarization curves and results. Therefore, the Al coatings provide excellent corrosion resistance for the S-NdFeB due to the formation of  $Al_2O_3$  oxide film.

#### Neutral Salt Spray (NSS) Tests

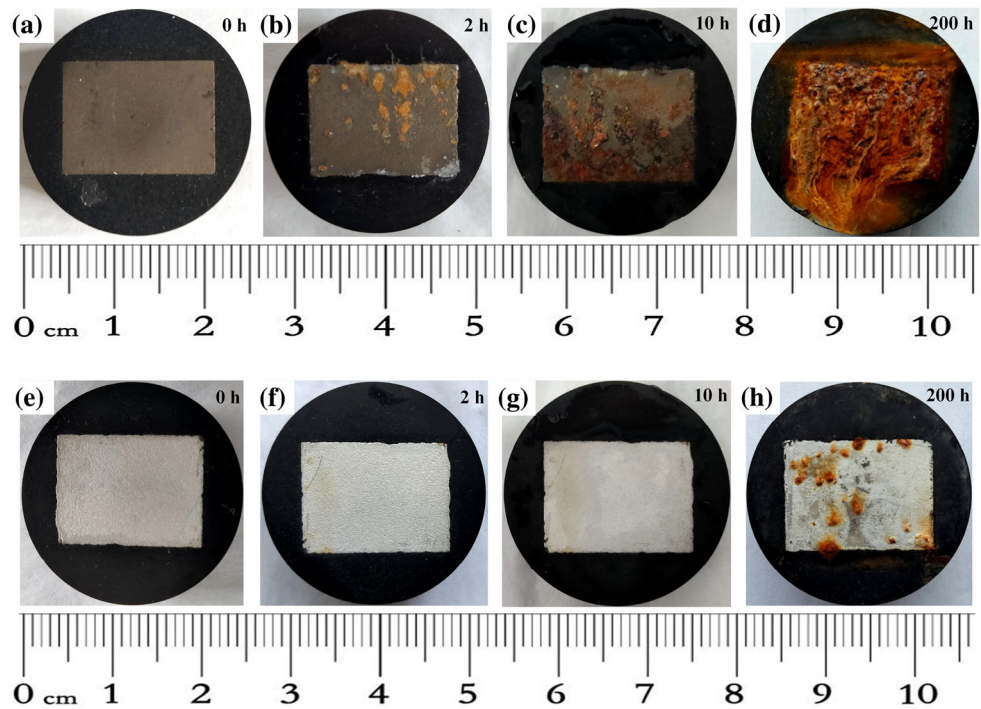
Figure 9 shows digital photos before and after the NSS tests for the S-NdFeB and Al-coated S-NdFeB. Before the salt spray test, as shown in Fig. 9(a) and (e), the surface of the S-NdFeB and Al-coated S-NdFeB are relatively flat without defects.

A little bit of red rust appeared on the surface of the S-NdFeB after NSS test for 2 h, as shown in Fig. 9(b), while a large area of red rust appeared on the surface of the S-NdFeB after NSS test for 10 h as shown in Fig. 9(c), which loosely covered the surface of the specimen. After NSS test for 200 h, the surface of the S-NdFeB has been

**Table 4** Electrochemical parameters obtained from equivalent circuit in Fig. 8 by simulation

Specimen	Immersion time, h	$R_{ss}$ , $\Omega \text{ cm}^2$	$Q_1$		$R_c$ , $\Omega \text{ cm}^2$	$Q_2$		$R_{ct}$ , $\Omega \text{ cm}^2$
			CPE, $Y_0$ (S-sec <sup>n</sup> )	$n$		CPE, $Y_0$ (S-sec <sup>n</sup> )	$n$	
Al/NdFeB	0	60.14	$3.098 \times 10^{-5}$	0.6134	21.21	$5.795 \times 10^{-7}$	0.9920	1877
Al/NdFeB	24	130.1	$2.359 \times 10^{-4}$	0.6551	305.5	$1.542 \times 10^{-4}$	0.7441	609.2
Al/NdFeB	48	77.03	$5.885 \times 10^{-4}$	0.6147	108	$2.684 \times 10^{-4}$	0.6614	984.9
Al/NdFeB	72	67.62	$9.022 \times 10^{-4}$	0.6120	103.8	$8.718 \times 10^{-4}$	0.6770	1691

**Fig. 9** Digital photos of the S-NdFeB and Al-coated S-NdFeB before and after the NSS tests: (a), (b), (c), (d) for S-NdFeB specimens; (e), (f), (g), (h) for Al-coated S-NdFeB.



completely covered by the red rust layer as shown in Fig. 9 (d), which is very thick, and part of it has been peeled off, indicating very serious corrosion.

The Al-coated S-NdFeB is intact after NSS test for 2 h and 10 h as shown in Fig. 9(f) and (g), respectively. After 200 h NSS test as shown in Fig. 9(h), a little bit of red rust appeared on the surface of the Al-coated S-NdFeB, and it indicates that the Al-coated S-NdFeB has superior corrosion resistance than the S-NdFeB.

The corrosion of metal materials by salt spray corrosion is mainly carried out by electrochemical method. The conductive salt solution ions penetrate into the interior of metal and set off local electrochemical reaction, and it forms “low potential metal (internal metal)—electrolyte solution (NaCl solution)—high potential impurity (surface corrosion product)” micro-battery system. Then, electrons transfer, anode metal dissolves, and forms new corrosion products (Ref 34). The surface of the S-NdFeB is porous,

and its rich Nd phase is easy to corrode,  $\text{Cl}^-$  quickly enters into the S-NdFeB and reacts with it during NSS test, resulting in S-NdFeB rust corrosion.

The radius of  $\text{Cl}^-$  is only  $1.81 \times 10^{-10}$  m, it has a strong penetration ability.  $\text{Cl}^-$  penetrates the oxide layer and protective layer, and it reacts electrochemically with the internal metal, resulting in material destruction. In addition,  $\text{Cl}^-$  is easily adsorbed in the pores and cracks of the metal surface.  $\text{Cl}^-$  pushes out and replaces the oxygen in the oxide layer, converts insoluble oxides into soluble chlorides, and turns inactive surfaces into active ones, thus causing the metal to be damaged (Ref 35). The Al coatings form an oxide film in air due to a long time of salt invasion, a large number of oxides convert into chloride, resulting in the final failure of the Al coatings.

Corrosion rates of the S-NdFeB and Al-coated S-NdFeB are calculated by the weight loss method. Weight losses of the S-NdFeB and Al-coated S-NdFeB after NSS tests are



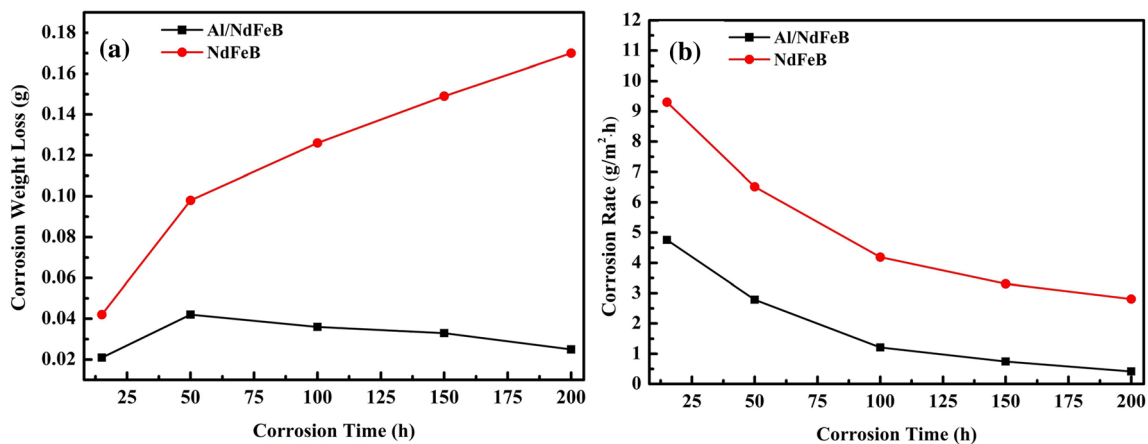


**Fig. 10** Weight losses (a) and corrosion rates (b) of the S-NdFeB and Al-coated S-NdFeB in NSS Tests

shown in Fig. 10(a). The weight loss of the S-NdFeB gradually increases with corrosion time due to continuous formation of the corrosion products on the surface of the S-NdFeB. Because the corrosion products are loose and porous, they have no protective effect on the S-NdFeB. The weight loss of Al-coated S-NdFeB increases first, and then decreases gradually with corrosion time, and it indicates that the chemical reaction of the Al coating decreases gradually in the later stage of corrosion.

The corrosion rates of the S-NdFeB and Al-coated S-NdFeB are shown in Fig. 10(b). The corrosion rates both of the S-NdFeB and Al-coated S-NdFeB are higher at the beginning of NSS test, and decrease rapidly and tend to be stable with increasing corrosion time. At the same time, the corrosion rates of the S-NdFeB are higher than that of the Al-coated S-NdFeB by over 95% in whole NSS test.

For the S-NdFeB, it is easy to quickly form a layer of corrosion products at the initial stage of reaction, and at the latter stage, the corrosion products formed in unit time are affected by corrosion products formed at the initial stage, with reduced corrosion rate.

The corrosion rates of the Al-coated S-NdFeB are half of the S-NdFeB at the initial stage of reaction, and oxide film formed on the surface of the Al-coated S-NdFeB effectively prevents salt fog ions from entering the interior of the coating, and avoids the deterioration of the corrosion. Therefore, corrosion rate of the Al-coated S-NdFeB tends to be stable at a later stage of NSS, with the accumulation of corrosion products, and oxide film on the surface of the Al-coated S-NdFeB is more compact. In the corrosion process of the Al-coated S-NdFeB, there will be no galvanic corrosion at the interface between the Al coating and the S-NdFeB. The corrosion rate of the Al coating is only 0.414 g/(m<sup>2</sup> h) after 200 h NSS test. Therefore, the Al coating can effectively protect the S-NdFeB from corrosion.

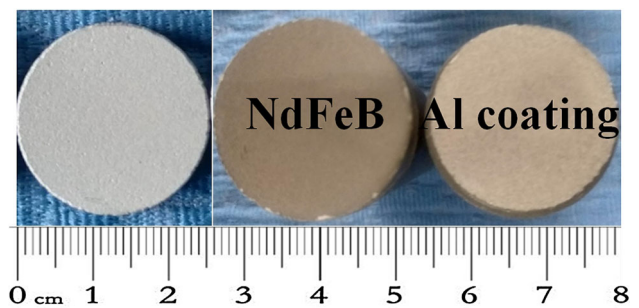


**Fig. 11** Morphologies of the Al-coated S-NdFeB before and after bonding strength test

### Mechanical Property

Mechanical properties measurements include bonding strength and hardness. Figure 11 shows the morphologies of the Al-coated S-NdFeB before and after bonding strength test. The Al coating is formed by colliding and stacking of high-speed Al particles during spraying, and the integrity of the coating is good. The Al coating is completely separated from the substrate after bonding strength test, and it indicates that the cohesive stress of the Al coating is higher than the bonding strength between the Al coating and the S-NdFeB.

Figure 12 shows the fracture surface microstructures of the Al coating detached from S-NdFeB after bonding strength test. It can be seen that fracture occurs inside the Al coating, and the failure mode of the coating is cohesive failure. There are two types of failure morphologies. Figure 12(a) shows that the failure surface of the coatings exists locally particles, and forms a loose porous structure. Figure 12(b) shows many cracks that can be observed from the failure surface of the coatings. The cracks will propagate along the direction of the applied load during bonding strength test, and the cracks will converge gradually with increasing load. When the larger longitudinal crack extends



**Fig. 12** Fracture surface microstructures of the Al coating detached from S-NdFeB after bonding strength test

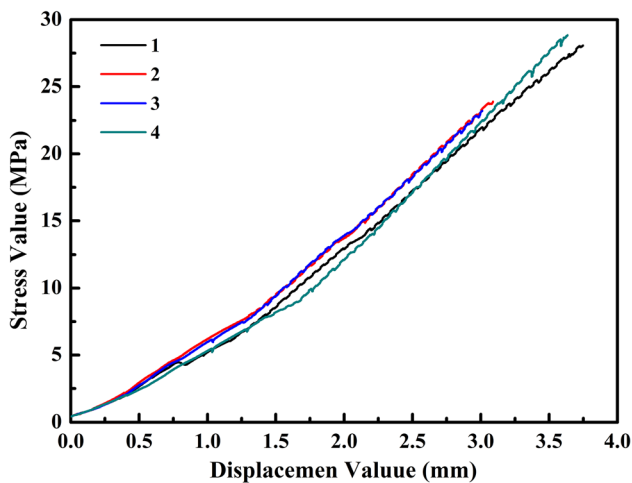
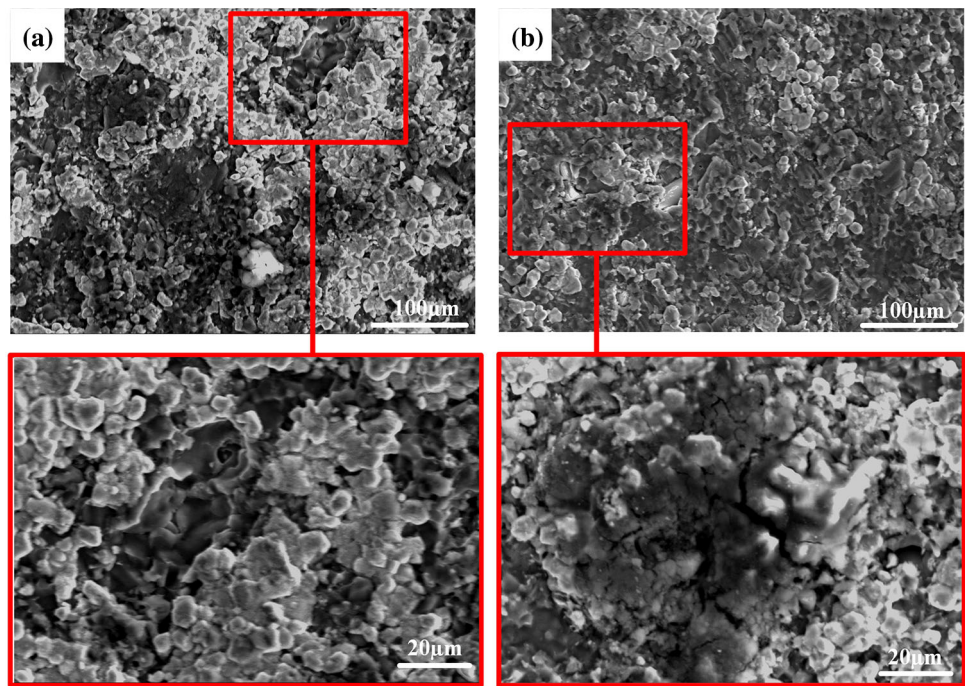


**Fig. 13** Stress–displacement curves of the Al-coated S-NdFeB

to the interface between the Al coating and the S-NdFeB, the transverse crack will occur at the interface, resulting in fracture of the Al-coated S-NdFeB. Loose porous structure of the coatings absorbs part of the energy through deformation, so it shows a certain toughness.

Figure 13 shows the stress–displacement curves of the Al-coated S-NdFeB. The stress increases gradually with an increase in vertical displacement, indicating that the Al coating is uniformly bonded with S-NdFeB.

Figure 14 shows the bonding strength and Vickers hardness of the Al-coated S-NdFeB, as well as Vickers hardness of the S-NdFeB. The average bonding strength and Vickers hardness of the Al-coated S-NdFeB are

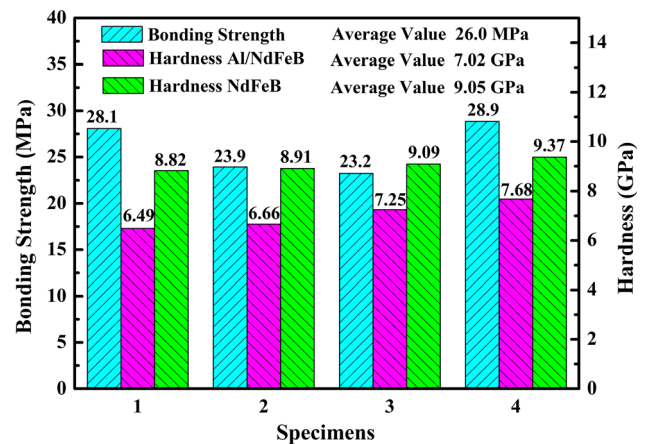


**Fig. 14** Bonding strength and Vickers hardness of the Al-coated S-NdFeB, Vickers hardness of the S-NdFeB

26.0 MPa and 7.02 GPa, respectively, whereas Vickers hardness of the S-NdFeB is 9.05 GPa.

Figure 15 shows indentation morphology of the Al-coated S-NdFeB. The indentation morphology of coatings are complete and regular rhombus; the indentation boundary is regular and clear, and it has obvious plastic deformation characteristics, which indicates that the coatings have a certain resistance to external load. Vickers hardness of the Al-coated S-NdFeB is lower than that of the S-NdFeB, and it also shows that the Al coating has a certain plastic deformation capacity. The bonding strength of Al coatings and NdFeB substrate is sufficient to meet the needs of NdFeB in practical work.

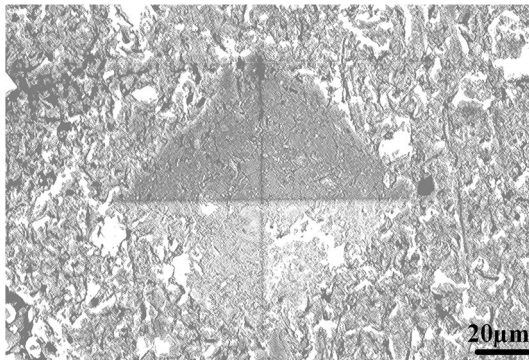


**Fig. 15** Indentation morphology of the Al-coated S-NdFeB

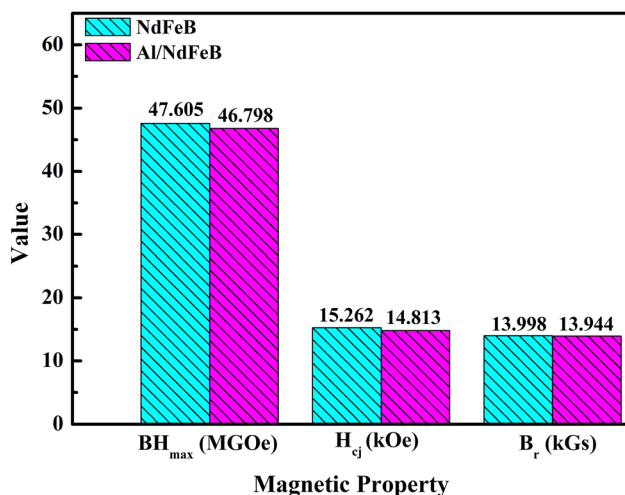


**Fig. 16** Magnetic properties of the S-NdFeB and Al-coated S-NdFeB

### Magnetic Property

Magnetic properties of the S-NdFeB and Al-coated S-NdFeB are tested by magnetic properties tester. Maximum magnetic energy product ( $BH_{max}$ ), intrinsic coercive field ( $H_{cj}$ ) and remanence ( $B_r$ ) are shown in Fig. 16. And demagnetization curve of the S-NdFeB and Al-coated S-NdFeB are shown in Fig. 17; all the three magnetic properties decrease less than 3% for the Al-coated S-NdFeB compared with the S-NdFeB. Because the Al coating is thin and the S-NdFeB is not hardly damaged in the spraying process, it has little effect on its magnetic properties, but with significant improvement of corrosion resistance.

### Conclusions

The dense Al coating with a thickness of 45  $\mu\text{m}$  was successfully prepared on the S-NdFeB by cold spray. Potentiodynamic curves and electrochemical impedance

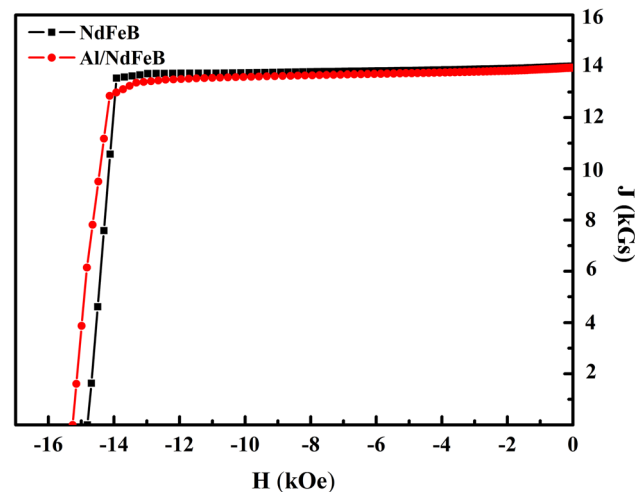


**Fig. 17** Demagnetization curve of the S-NdFeB and Al-coated S-NdFeB

spectroscopy in 3.5 wt.% NaCl solution revealed that the Al-coated S-NdFeB can survive up to 200 h in the neutral salt spray test (NSS). The cold-sprayed Al coatings could improve the corrosion resistance of the sintered NdFeB magnets and provide long-time protection to the NdFeB substrate due to the formation of  $\text{Al}_2\text{O}_3$  oxide film. The Al coatings have a bonding strength and a Vickers hardness of 26.0 MPa and 7.02 GPa, respectively. Moreover, the loss of maximum magnetic energy product ( $BH_{max}$ ), intrinsic coercive field ( $H_{cj}$ ) and remanence ( $B_r$ ) of the Al-coated S-NdFeB compared with the S-NdFeB is less than 3%. Therefore, the cold spray is an economically viable, environmentally friendly, and feasible method to protect the sintered NdFeB magnets from corrosion by depositing Al coating.

**Acknowledgments** This work is supported by the National Natural Science Foundation of China (Nos. 52062040, 51865044, 52062041), Science and Technology Projects of Inner Mongolia Autonomous Region (2018-810, 2019-1356). The authors are grateful to Dr. Xueping Zhao, Dr. Xiaohu Hou and Dr. Fei Liu from the analysis and test center of Inner Mongolia University of technology for their testing help.

### References

1. H. Chen, X. Yang, L. Sun, P. Yu, X. Zhang, and L. Luo, Effects of Ag on the Magnetic and Mechanical Properties of Sintered NdFeB Permanent Magnets, *J. Magn. Magn. Mater.*, 2019, **485**, p 49-53.
2. M. Sagawa, S. Fujimura, N. Togawa, H. Yamamoto, and Y. Matsuura, New Material for Permanent Magnets on a Base of Nd and Fe, *J. Appl. Phys.*, 1984, **55**, p 2083-2087.
3. L.Z. Song, Y.A. Wang, W.Z. Lin, and Q. Liu, Primary Investigation of Corrosion Resistance of Ni-P/TiO<sub>2</sub> Composite Film on Sintered NdFeB Permanent Magnet, *Surf. Coat. Technol.*, 2008, **202**(21), p 5146-5150.

4. Y.W. Song, H. Zhang, H.X. Yang, and Z.L. Song, A Comparative Study on the Corrosion Behavior of NdFeB Magnets in Different Electrolyte Solutions, *Mater. Corros.*, 2008, **59**(10), p 794-801.
5. D.F. Cygan and M.J. McNallan, Corrosion of NdFeB Permanent Magnets in Humid Environments at Temperatures up to 150 °C, *J. Magn. Magn. Mater.*, 1995, **1**(1-2), p 131-138.
6. G.W. Warren, G. Gao, and Q. Li, Corrosion of NdFeB Permanent Magnet Materials, *J. Appl. Phys.*, 1991, **70**(10), p 6609-6611.
7. Q.J. He and W. Li, 钕铁硼永磁材料防腐蚀研究进展 (Progress in Research on Anticorrosion of NdFeB Permanent Magnet), *Met. Funct. Mater.*, 2001, **8**(5), p 8-13. ((in Chinese)).
8. Q.L. Yuan, J.J. Cao, and Z.J. Su, 烧结型NdFeB永磁体的防腐蚀研究进展 (Progress in Research on Anticorrosion of Sintered Type Neodymium Iron Boron), *Surf. Technol.*, 2008, **38**(1), p 76-78. ((in Chinese)).
9. W.Q. Liu, M. Yue, J.X. Zhang, and G.P. Wang, 烧结NdFeB永磁合金本征腐蚀特性研究进展 (Intrinsic Corrosion Characteristic of Sintered NdFeB Permanent Magnets), *Powder Metall. Technol.*, 2006, **24**(3), p 195-198. ((in Chinese)).
10. Z. Chen, J.Z. Alicen, X.F. Yi, and F. Chen, Multi-Layered Electroless Ni-P Coatings on Power-Sintered NdFeB Permanent Magnet, *J. Magn. Magn. Mater.*, 2006, **302**(1), p 216-222.
11. E. Chen, K. Peng, W.L. Yang, J.J. Zhu, D.Y. Li, and L.P. Zhou, Effects of Al Coating on Corrosion Resistance of Sintered NdFeB Magnet, *Trans. Nonferr. Met. Soc. China*, 2014, **24**(9), p 2864-2869.
12. W.C. Lang, B. Gao, W. Chen, and B.Z. Wu, 高性能工具镀层及其制备技术概括与进展 Overview and Progress of High Performance Tool Coating and Its Preparation Technology, *J. Wenzhou Voca. Technol. Colg.*, 2015, **15**(1), p 50-54, 58 ((in Chinese)).
13. T.T. Xie, S.D. Mao, C. Yu, S.J. Wang, and Z.L. Song, Structure, Corrosion and Hardness Properties of Ti/Al Multilayers Coated on NdFeB by Magnetron Sputtering, *Vacuum*, 2012, **86**(10), p 1583-1588.
14. J.L. Li, S.D. Mao, K.F. Sun, X.M. Li, and Z.L. Song, AlN/Al Dual Protective Coatings on NdFeB by DC Magnetron Sputtering, *J. Magn. Magn. Mater.*, 2009, **321**(22), p 3799-3803.
15. S.D. Mao, H.X. Yang, J.L. Li, F. Huang, and Z.L. Song, Corrosion Properties of Aluminium Coatings Deposited on Sintered NdFeB by Ion-Beam-Assisted Deposition, *Appl. Surf. Sci.*, 2011, **257**(13), p 5581-5585.
16. W.Y. Li, X.P. Guo, C. Verdy, L. Dembinski, H.L. Liao, and C. Coddet, Improvement of Microstructure and Property of Cold-Sprayed Cu-4at.%Cr-2at.%Nb Alloy by Heat Treatment, *Scr. Mater.*, 2006, **55**(4), p 327-330.
17. B. Dikici, H. Yilmazer, I. Ozdemir, and M. Isik, The Effect of Post-Heat Treatment on Microstructure of 316L Cold-Sprayed Coatings and Their Corrosion Performance, *J. Therm. Spray Technol.*, 2016, **25**(4), p 704-714.
18. B. Dikici and M. Topuz, Production of Annealed Cold-Sprayed 316L Stainless Steel Coatings for Biomedical Applications and Their in-vitro Corrosion Response, *Prot. Met. Phys. Chem. Surf.*, 2018, **54**(2), p 333-339.
19. A.P. Alkhimov, V.F. Kosarev, and A.N. Papyrin, Gas-Dynamic Spraying, an Experimental Study of the Spraying Process, *J. Appl. Mech. Tech. Phys.*, 1998, **39**(2), p 318-323.
20. V.K. Champagne, D.J. Helfritch, and P.F. Leyman, Magnesium Repair by Cold Spray, *Plat. Surf. Finish.*, 2008, **95**(9), p 19-28.
21. Y.S. Tao, T.Y. Xiong, C. Sun, H. Jin, H. Du, and T.F. Li, Effect of  $\alpha$ -Al<sub>2</sub>O<sub>3</sub> on the Properties of Cold Sprayed Al/ $\alpha$ -Al<sub>2</sub>O<sub>3</sub> Composite Coatings on AZ91D Magnesium Alloy, *Appl. Surf. Sci.*, 2009, **256**(1), p 261-266.
22. S. Kuroda, J. Kawakita, and M. Takemoto, An 18-Year Exposure Test of Thermal-Sprayed Zn, Al and Zn-Al Coatings in Marine Environment, *Corrosion*, 2006, **62**(7), p 635-647.
23. T.C. Chen, C.C. Chou, T.Y. Yung, K.C. Tsai, and J.Y. Huang, Wear Behavior of Thermally Sprayed Zn/15Al, Al and Inconel 625 Coatings on Carbon Steel, *Surf. Coat. Technol.*, 2016, **303** (Part A), p 78-85.
24. Y.X. Liu and J.X. Wen, 绿色缓蚀剂对金属铝的缓蚀性能研究进展 (Research Progress of Green Corrosion Inhibitor for Aluminium), *Guangzhou Chem. Ind.*, 2019, **47**(12), p 27-28. ((in Chinese)).
25. Z.L. Song, 钕铁硼永磁材料腐蚀和防护研究进展 (Research Progress on Corrosion and Protection of NdFeB Permanent Magnetic Materials), **8**, p 118-128 ((in Chinese)).
26. S.Z. Song and Z.L. Tang, An Electrochemical Impedance Analysis on Al in 3.5% NaCl Solution, *J. Chin. Soc. Corros. Prot.*, 1996, **16**(2), p 127-132.
27. C.C. Ma, X.F. Liu, and C.G. Zhou, Cold-Sprayed Al Coating for Corrosion Protection of Sintered NdFeB, *J. Therm. Spray Technol.*, 2013, **23**(3), p 456-462.
28. M. Yue, J.X. Zhang, W.Q. Liu, and G.P. Wang, Corrosion Kinetics of Spark Plasma Sintering Nd-Fe-B Magnets in Different Electrolytes, *IEEE Tran. Magn.*, 2005, **41**(10), p 3892-3894.
29. Y.S. Huang, X.T. Zeng, X.F. Hu, and F.M. Liu, Corrosion Resistance Properties of Electroless Nickel Composite Coatings, *Electrochim. Acta*, 2004, **49**(25), p 4313-4319.
30. E. Barsoukoff and J.R. Macdonald, *Impedance Spectroscopy Theory, Experiment, and Application*, 2nd ed. Wiley, Hoboken, 2005.
31. J.B. Bessone, D.R. Salinas, C.E. Mayer, M. Ebert, and W.J. Lorenz, An EIS Study of Aluminium Barrier-Type Oxide Films Formed in Different Media, *Electrochim. Acta*, 1992, **37**(12), p 2283-2290.
32. J.F. Zhang, W. Zhang, C.W. Yan, K.Q. Du, and F.H. Wang, Corrosion Behaviors of Zn-Al-Mn Alloy Composite Coatings Deposited on Magnesium Alloy AZ31B (Mg-Al-Zn), *Electrochim. Acta*, 2009, **55**(2), p 560-571.
33. H. Zhang, Y.L. Zhao, and Z.D. Jiang, Effects of Temperature on the Corrosion Behavior of 13Cr Martensitic Stainless Steel During Exposure to CO<sub>2</sub> and Cl<sup>-</sup> Environment, *Mater. Lett.*, 2005, **59**(27), p 3370-3374.
34. J.H. Xu, 盐雾试验及盐雾试验箱应用技术基础 (Salt Spray Test and Salt Spray Test Chamber Application Technology Foundation), *National Defence Industry Press*, 1993, p 27-40 ((in Chinese)).
35. Y.L. Lu and M.X. Cao, 中性盐雾试验影响因素探讨 (Discussion on the Influence Factor of Neutral Salt Spray Test), *Meishan Technol.*, 2012, **1**(1), p 56-58. ((in Chinese)).

#### Publisher's Note

Springer Nature remains neutral with regard to jurisdictional claims in published maps and institutional affiliations.